The effect of buttressing on grounding line dynamics

Supplementary online material

Marianne HASELOFF[1] and Olga V. SERGIENKO[1]

March 6, 2018

S-1 Boundary layer at the calving front

The purpose of this section is to show that using the first order boundary condition (8b) together with the zeroth order momentum balance (17a) gives the same result as the introduction of a boundary layer at the calving front, and is therefore consistent with our use of matched asymptotic expansions. As pointed out by Hindmarsh (2012), the mathematical problem (7a)–(8b) is fully analogous to the boundary layer problem at the grounding line considered in Schoof (2007), with the basal friction term $|u|^{m-1}u$ in Schoof (2007) replaced with the lateral friction term $h|u|^{p-1}u$. In Schoof's problem, the ice thickness at the grounding line is known, but the flux is a higher-order correction. Here, we know the ice flux at the calving front $q_1 = 1 + \dot{m}$ from (9), and we want to determine the ice thickness at the calving front. The other difference between our problem and that in Schoof (2007) is that the we are not considering a singular perturbation problem, but a regular one: equations (17a)–(17c) are well-posed already, and can be solved without the first order correction.

Following Schoof (2007), we rescale (7a)–(8b) at the calving front with

$$x = 1 - \eta^a \tilde{X}, \qquad \tilde{h} = \eta^b \tilde{H}, \qquad \tilde{u} = \eta^c \tilde{U}. \tag{S-1}$$

Mass continuity ($\tilde{u}\tilde{h} \sim \tilde{U}\tilde{H}$), requires $b = -c$. Balancing the different terms in the momentum balance (7a) further yields

$$a = \frac{n(1+p)}{2+n+p}, \qquad b = \frac{n}{n+p+2}. \tag{S-2}$$

With these scales, and ignoring terms of $O(\eta^{n(1+p)/2+n+p})$, the mass balance identity (9) becomes

$$\tilde{U}\tilde{H} = 1 + \dot{m} \tag{S-3a}$$

[1] *AOS Program, Princeton University, Princeton, NJ, USA*

Correspondence: Marianne Haseloff, <marianne.haseloff@earth.ox.ac.uk>

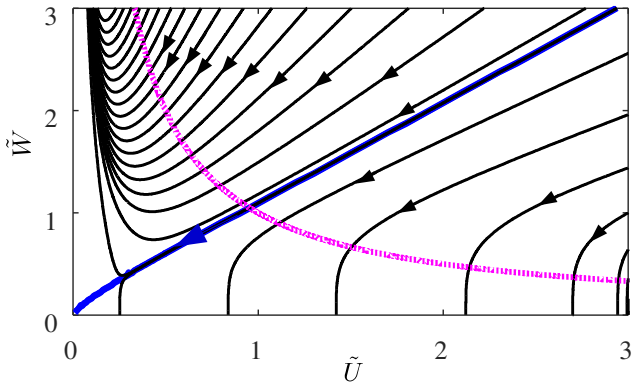

Figure S-1: Phase plane of calving front boundary layer equations for $n = 1/p = 3$ and $\beta = 0.5$, $Q = 1.0$. Arrows indicate the direction of increasing $\tilde{X}$. Magenta line: $\tilde{W} = Q/U$, the boundary condition given by (S-4c).

and the boundary layer momentum balance equation is the scaled version of (7a)

$$\frac{\partial}{\partial \tilde{X}} \left(\tilde{H} \left| \frac{\partial \tilde{U}}{\partial \tilde{X}} \right|^{1/n-1} \frac{\partial \tilde{U}}{\partial \tilde{X}} \right) - \beta \tilde{H} |\tilde{U}|^{p-1} \tilde{U} + 2\tilde{H} \frac{\partial \tilde{H}}{\partial \tilde{X}} = 0 \qquad \text{on} \quad \tilde{X} \in (0, \infty) \tag{S-3b}$$

with the boundary conditions

$$\left.\begin{aligned} \tilde{H} &= \tilde{H}_1 \\ \tilde{H} \left| \frac{\partial \tilde{U}}{\partial \tilde{X}} \right|^{1/n-1} \frac{\partial \tilde{U}}{\partial \tilde{X}} &= -\tilde{H}^2 \end{aligned}\right\} \qquad \text{at } \tilde{X} = 0 \tag{S-3c}$$

and the matching conditions

$$\left.\begin{aligned} \tilde{U} &\sim \eta^{\frac{n}{2+p+n}} \tilde{u} \\ \tilde{H} &\sim \eta^{\frac{-n}{2+p+n}} \tilde{h} \\ \tilde{U}\tilde{H} &\sim \tilde{u}\tilde{h} \end{aligned}\right\} \qquad \text{as } \tilde{X} \to \infty,\ x \to 1. \tag{S-3d}$$

Mathematically, we have now arrived at an initial value problem with the initial values given by (S-3c), and the far field conditions given by (S-3d). At this point, we do not know what the correct choice of H_1 is, but we know that it has to be chosen in such a way that the far field velocity and ice thickness satisfy the matching conditions (S-3d). We can illustrate this by defining $Q = \tilde{U}\tilde{H} = 1 + \dot{m}$ and $\partial\tilde{U}/\partial\tilde{X} = -|\tilde{W}|^{n-1}\tilde{W}$ to re-formulate (S-3) as (compare Schoof, 2007)

$$\frac{\partial \tilde{U}}{\partial \tilde{X}} = -|\tilde{W}|^{n-1}\tilde{W} \tag{S-4a}$$

$$\frac{\partial \tilde{W}}{\partial \tilde{X}} = 2\frac{Q|\tilde{W}|^{n-1}\tilde{W}}{\tilde{U}^2} - \beta|\tilde{U}|^p - \frac{|\tilde{W}|^{n+1}}{\tilde{U}} \tag{S-4b}$$

with the 'initial' conditions

$$\tilde{W} = H_1, \qquad \tilde{U} = \frac{Q}{H_1} \qquad \text{at } \tilde{X} = 0 \tag{S-4c}$$

and far field conditions

$$\tilde{W} \to 0, \qquad \tilde{U} \to 0 \qquad \text{as } \tilde{X} \to \infty. \tag{S-4d}$$

Figure S-1 shows a phase plane diagram of (S-4a)–(S-4d). The initial condition (S-4c) is plotted as dotted magenta line, and solutions of (S-4a)–(S-4b) orginating from different initial conditions are plotted as black lines with the arrow indicating increasing $\tilde{X}$. It is apparent that all but one solutions diverge for $\tilde{X} \to \infty$. The one trajectory (the bold blue line) which satisfies both the initial conditions (equation (S-4c), dashed magenta line) and the far-field conditions (S-4d) is the desired solution, and the value of W at the intersection of this trajectory with the initial condition (magenta line) determines the unknown initial condition H_1 according to $(\text{S-4c})_1$.

Similar to the grounding line problem in Schoof (2007), no general closed-form solution of (S-3) exists for $n \neq 1$, $p \neq 1$ and we repeat the same steps as Schoof (2007) to derive an approximate local solution based on the assumption that $\tilde{U}$ and $\tilde{W} = -|\partial\tilde{U}/\partial\tilde{X}|^{1/n-1}\partial\tilde{U}/\partial\tilde{X}$ are small. In this case, we can approximate the solution to (S-3) with a local solution $\tilde{W} \sim C\tilde{U}^{\nu}$, which substituted into (S-4b) gives:

$$\frac{\partial\tilde{W}}{\partial\tilde{X}} = 2C^n Q|\tilde{U}|^{\nu(n-1)+\nu-2} - \beta|\tilde{U}|^p - C|\tilde{U}|^{\nu(n+1)-1} \tag{S-5}$$

Balancing the first and second term on the right-hand side of (S-5) yields $\nu = (2+p)/n$ and $C = (\beta/(2Q))^{1/n}$. With these choices, the third term on the right-hand side of (S-5) is of $O(U^{p+1+(2+p)/n})$ and therefore small in comparison to the first two terms. Applying the initial conditions (S-4c), we obtain for the scaled ice thickness at the calving front

$$H_1 = \left(\frac{\beta}{2}Q^{1+p}\right)^{\frac{1}{2+n+p}}. \tag{S-6}$$

As $\tilde{h} = \eta^{n/(n+p+2)}H$ and $Q = 1 + \dot{m}$, this yields for the ice thickness at the calving front

$$h_1 = \left(\eta^n \frac{\beta}{2}(1+\dot{m})^{1+p}\right)^{\frac{1}{2+n+p}}, \tag{S-7}$$

which is the same as (19).

S-2 Ice thickness at the calving front

In this section, we compare our ad-hoc approximation of the ice thickness at the calving front (31) with an exact solution for $n = p = 1$ and $\dot{m} = 0$ by Pegler (2016). In this case, Pegler (2016) finds:

$$h_{1,\text{exact}} = \frac{1}{\sqrt{\sqrt{\frac{\pi}{\beta\eta}}\text{erf}\left(\sqrt{\frac{\beta}{\eta}}\right) + \exp\left(-\frac{\beta}{\eta}\right)}}. \tag{S-8}$$

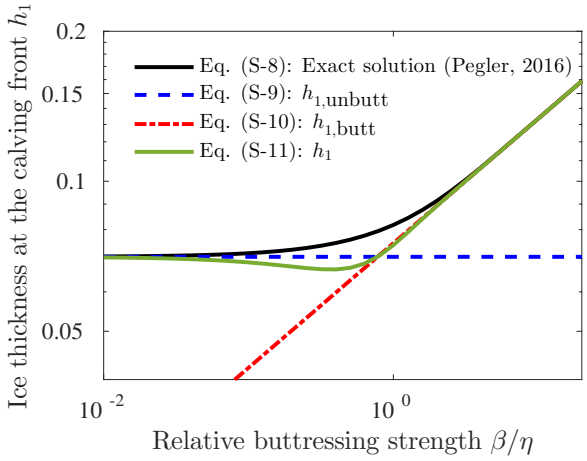

Figure S-2: Same as figure 4, but for $n = p = 1$ and $\dot{m} = 0$. $h_{1,\mathrm{butt}}$ is the asymptotic solution for buttressed ice shelves (S-10), $h_{1,\mathrm{unbutt}}$ is the exact solution for unconfined ice shelves (S-9), h_1 is the approximate solution (S-11), and $h_{1,\mathrm{exact}}$ is the exact solution by Pegler (2016), equation (S-8). $\eta = 10^{-2}$.

The ice thickness expression for unbuttressed ice shelves (32) can be recovered from (S-8) by introducing a series expansion of $\mathrm{erf}(\sqrt{\beta/\eta})$ for small $\sqrt{\beta/\eta}$:

$$h_{1,\mathrm{unbutt}} = \sqrt{\frac{\eta}{\eta + 2}}, \tag{S-9}$$

For $n = 1$, the boundary layer problem at the calving front (section S-1) can be solved exactly, which leads to a slightly modified result (see also Pegler, 2016)

$$h_{1,\mathrm{butt}} = \left(\frac{\beta\eta}{\pi}\right)^{1/4} \tag{S-10}$$

which agrees with the exact solution (S-8) in the limit of $\beta \gg \eta$, i.e., for strongly buttressed ice shelves. Finally, our approximate solution (31) gives:

$$h_1^4 = h_{1,\mathrm{butt}}^4 \mathrm{erf}\left(\frac{\beta}{\eta}\right) + h_{1,\mathrm{unbutt}}^4 \mathrm{erfc}\left(\frac{\beta}{\eta}\right). \tag{S-11}$$

Figure S-2 compares the performance of (S-11) with Pegler's exact solution (S-8). As for $n = 1/p = 3$, the approximate solution correctly captures the two asymptotic limits, but does not match $h_{1,\mathrm{exact}}$ in the transition zone between the two.

S-2.1 Grounding line positions for thickness-based calving laws

We now compare the performance of our approximate solution (S-11) with the exact solution (S-8) in predictions of the grounding line position. For $m = n = p = 1$ and $\dot{m} = 0$, the ice flux at the grounding line is given by (16):

$$q_g = \left[\frac{A(\rho g)^2(1-\rho/\rho_w)}{C} h_g^5 + \left(\frac{\rho g L_s}{CW^2} h_g^3\right)^2\right]^{1/2} - \frac{\rho g L_s}{CW^2} h_g^3, \tag{S-12}$$

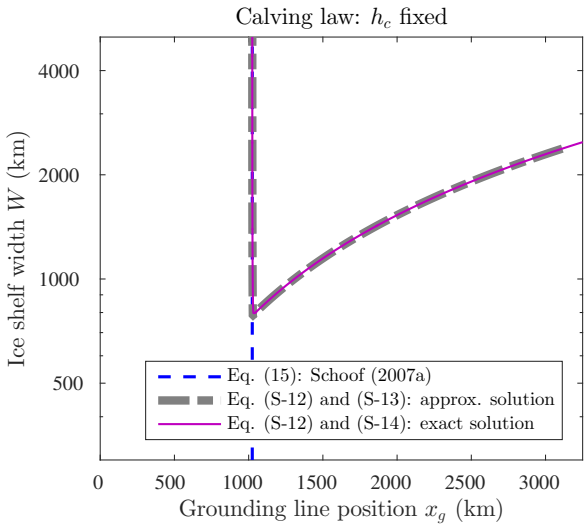

Figure S-3: Same as figure 7 but for a linearized version with $n = m = p = 1$ and $\dot{m} = 0$. Calving occurs when the ice thickness at the calving front is less than a critical ice thickness. Ice shelf widths are plotted vs grounding line position. Grounding line positions are calculated by solving $\dot{a}x_g = q_g$ (47) with (S-12) and either (S-13) or (S-14). The solutions obtained with the approximate ice thickness expression (S-14) agree well with the solutions obtained with the exact ice thickness expression (S-13). We used $A = 1.67 \times 10^{-10}$ Pa^{-1} s^{-1} and $C = 7.624 \times 10^2$ Pa m^{-1} s.

where we used the formula by Hindmarsh (2012) to determine Λ. The dimensional form of (S-11) is

$$h_{c,\text{exact}} = \left[\sqrt{\frac{\pi}{2}} \frac{\rho g \left(1 - \frac{\rho}{\rho_w}\right) AW}{4 q_g} \text{erf}\left(\sqrt{2}\frac{L_s}{W}\right) + \frac{1}{h_g^2} \exp\left(-2\frac{L_s^2}{W^2}\right) \right]^{-1/2} . \tag{S-13}$$

The approximate ice thickness is given by

$$h_c = \left[h_{c,\text{unbutt}}^4 \text{erfc}\left(\sqrt{2}\frac{L_s^2}{W^2}\right) + h_{c,\text{butt}}^4 \text{erf}\left(\sqrt{2}\frac{L_s^2}{W^2}\right) \right]^{1/4} \tag{S-14}$$

with

$$h_{c,\text{unbutt}} = \frac{h_g}{\left[1 + \frac{1}{2q_g} A\rho g (1 - \frac{\rho}{\rho_w}) L_s h_g^2\right]^{\frac{1}{2}}} \tag{S-15a}$$

$$h_{c,\text{butt}} = 2\left(\frac{2}{\pi}\right)^{1/4} \left[\frac{q_g}{\rho g \left(1 - \frac{\rho}{\rho_w}\right) AW} \right]^{1/2} \tag{S-15b}$$

Figure S-3 shows grounding line positions for different ice shelf widths obtained from solving (47) with (S-12) and either (S-13) or (S-14) with a fixed ice thickness at the calving front. The two solutions agree very well. As in the example in figure 7, there are two branches, which connect at a minimum width. The stabilty of these two branches can again be inferred from (50), which confirms that the left branch (which predicts grounding line positions close to the unbuttressed solution) is stable, while the other branch is unstable.

References

R. C. A. Hindmarsh. An observationally validated theory of viscous flow dynamics at the ice-shelf calving front. *Journal of Glaciology*, 58(208):375–387, 2012. doi: 10.3189/2012JoG11J206.

S. S. Pegler. The dynamics of confined extensional flows. *Journal of Fluid Mechanics*, 804:24–57, 2016.

C. Schoof. Marine ice-sheet dynamics. Part 1. The case of rapid sliding. *Journal of Fluid Mechanics*, 573:27–55, 2007. doi: 10.1017/S0022112006003570.